

Understanding Nonlinear Dielectric Properties in a Biaxially Oriented Poly(vinylidene fluoride) Film at Both Low and High Electric Fields

Yue Li,^{†,‡} Janet Ho,[§] Jianchuan Wang,^{*,†,⊥} Zhong-Ming Li,[†] Gan-Ji Zhong,[†] and Lei Zhu^{*,†}

[†]College of Polymer Science and Engineering, State Key Laboratory of Polymer Materials Engineering, Sichuan University, Chengdu 610065, Sichuan, P. R. China

[‡]Department of Macromolecular Science and Engineering, Case Western Reserve University, Cleveland, Ohio 44106-7202, United States

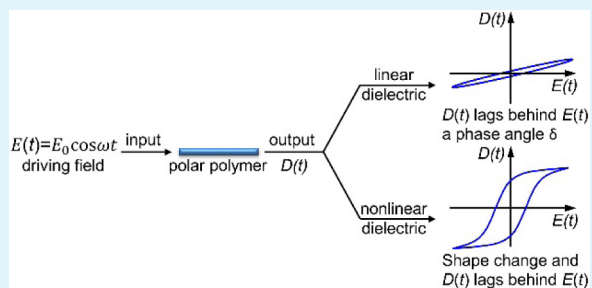
[§]Army Research Laboratory, RDRL-SED-C, 2800 Powder Mill Road, Adelphi, Maryland 20783, United States

[⊥]College of Chemistry and Chemical Engineering, Chongqing University, Chongqing 400044, P. R. China

Supporting Information

ABSTRACT: Understanding nonlinear dielectric behavior in polar polymers is crucial to their potential application as next generation high energy density and low loss dielectrics. In this work, we studied nonlinear dielectric properties of a biaxially oriented poly(vinylidene fluoride) (BOPVDF) film under both low and high electric fields. For fundamental nonlinear dielectric constants at low fields (<30 MV/m), Novocontrol high-voltage broadband dielectric spectroscopy (HVBDS) was accurate enough to measure up to the third harmonics. It was observed that the low-field dielectric nonlinearity for the BOPVDF disappeared above 10 Hz at room temperature, suggesting that the low-field dielectric nonlinearity originated from ionic migration of impurity ions rather than dipolar relaxation of the amorphous segments. Above the coercive field ($E_C \approx 70$ MV/m), bipolar electric displacement-electric field ($D-E$) loop tests were used to extract the nonlinear behavior for pure PVDF crystals, which had a clear origin of ferroelectric switching of polar crystalline dipoles and domains and nonpolar-to-polar ($\alpha \rightarrow \delta \rightarrow \beta$) phase transformations. By using HVBDS, it was observed that the ferroelectric switching of polar crystalline dipoles and domains in BOPVDF above the E_C always took place between 20 and 500 Hz regardless of a broad range of temperature from -30 to 100 °C. This behavior was drastically different from that of the amorphous PVDF dipoles, which had a strong dependence on frequency over orders of magnitude.

KEYWORDS: *poly(vinylidene fluoride), ferroelectric, nonlinear dielectric property, high-voltage broadband dielectric spectroscopy, dipolar relaxation*



INTRODUCTION

Polymer dielectrics find numerous practical and potential applications, including film capacitors,^{1,2} gate dielectrics for organic electronics,^{3,4} dielectric elastomers,^{5,6} electrostriction,^{7,8} and electrocaloric cooling,^{9,10} due to their stable capacitance, low dielectric loss, high dielectric breakdown strength, and long lifetime. In practical applications such as DC-link capacitors for electric vehicles,^{11,12} the operation electric field is often as high as 200–300 MV/m. Under such high electric fields, nonlinear dielectric properties can become significant and thus are detrimental to their electrical performance because nonlinear harmonics contribute significantly to dielectric losses. Therefore, it is of great importance to understand nonlinear dielectric properties for polymers at both low and high electric fields.

Because of limited experimental techniques for high-field and high-frequency switching,¹³ the exact molecular origin and mechanisms for nonlinear dielectric behavior in polymers has not been well-understood. Several physical events in dielectric polymers are considered as possible sources for nonlinear

dielectric properties. First, dielectric relaxation processes associated with the micro-Brownian motion of dipoles in the amorphous segments (i.e., multiple repeat units) of polar polymers are considered as a source for nonlinear dielectric properties. In particular, when the test frequency overlaps with the primary dipolar relaxation (i.e., glass transition) peak, the nonlinear dielectric constants can reach significant values. Examples include poly(vinyl acetate) (PVAc),^{14,15} poly(vinylidene cyanide-*alt*-vinyl acetate) (P(VDCN-VAc)),^{14,16} and dipolar dye (Disperse Red 1)-doped glassy polymers near and slightly above their glass transition temperatures (T_g).¹⁷ Second, ferroelectric switching and phase transitions (e.g., Curie transition) are considered as the second source of nonlinear dielectric behavior. For example, semicrystalline poly(vinylidene fluoride) (PVDF) and P(VDF-*co*-trifluoro-

Received: October 3, 2015

Accepted: December 23, 2015

Published: December 23, 2015

ethylene) (P(VDF-TrFE)) copolymers exhibit significant nonlinear ferroelectric switching above the coercive field (E_C).^{18–20} Similarly, ferroelectric liquid crystals and polymers are also reported to show nonlinear dielectric properties primarily due to ferroelectric switching.^{21,22} Around the Curie transition temperature (T_C), P(VDF-TrFE) copolymers exhibit considerable nonlinear dielectric behavior.^{20,23} Third, electronic or ionic conduction could be another source of nonlinear dielectric properties. However, there are limited reports on this subject. For example, it is proposed that hole-hopping between neighboring *p*-type SiC nanoparticles in a silicone rubber matrix could be the origin of nonlinear electric property of the nanocomposite.²⁴

From the above review, it is seen that nonlinear dielectric properties are closely related to the primary relaxation processes in polar, rather than nonpolar, polymers, which are promising to achieve high dielectric constant, high energy density, and low loss dielectric properties, as discussed in a recent perspective article.¹ It is necessary to understand various mechanisms of nonlinear dielectric behavior in polar polymers to achieve low dielectric losses. In this study, we discuss viable experimental techniques for an accurate measurement of nonlinear dielectric properties at both low and high electric fields. Two major techniques are compared, namely, high-voltage broadband dielectric spectroscopy (HVBDS, developed by Novocontrol) is accurate for low-field nonlinear dielectricity (i.e., for fundamental nonlinear dielectric constants), and electric displacement–electric field (D – E) loop tests are suitable for high-field nonlinear dielectricity (i.e., for apparent nonlinear dielectric constants). A commercial biaxially oriented PVDF (BOPVDF) film (8 μm) with 54 wt % crystallinity (70% α and 30% β phases) is used for this study. It is observed that dipolar relaxation of amorphous PVDF dipoles is not the source of nonlinear dielectric behavior at low fields (i.e., below the E_C) because the dipolar relaxation frequency is as high as 1 MHz at room temperature. Instead, ionic conduction from impurity ions in the sample is the major source of nonlinear dielectric behavior. At high fields (i.e., above the E_C), ferroelectric switching of β dipoles/domains in PVDF crystals and electric field-induced $\alpha \rightarrow \beta$ phase transformation are the major sources of nonlinear dielectric properties. Our improved understanding of nonlinear dielectric properties in polar polymers such as BOPVDF will help us design viable approaches to utilize polar polymers for high energy density and low loss dielectrics. For example, multilayer polymer films are effective to minimize nonlinear dielectric behavior of PVDF and its copolymers at both low and high electric fields.^{25–27}

EXPERIMENTAL SECTION

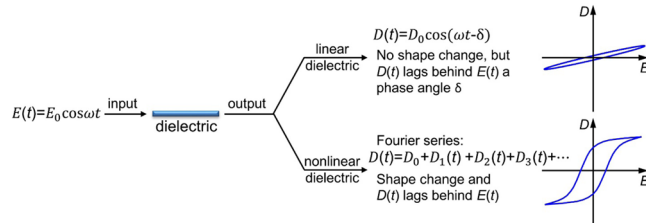
Materials. The BOPVDF film was obtained from Kureha Corporation (Tokyo, Japan). As recently reported,²⁸ the crystallinity was about 54 wt % (or 48 vol %), and the crystalline phase contained 70% α and 30% β crystals. The film thickness was uniform at 8.0 μm . Fresh film samples were thoroughly dried in a vacuum oven for 3 days before any tests.

Instruments and Characterization. HVBDS measurements were performed on a Novocontrol Concept 80 broadband dielectric spectrometer with a high-voltage interface, HVB4000. The interface could provide ± 2000 V high voltage with frequency up to 10⁴ Hz. Complex relative permittivity could be measured with and without high harmonics. Around 50 nm thick Au electrodes were evaporated using electron beam (EvoVac Deposition System, Angstrom Engineering, Inc.) onto both sides of the film sample, and the electrode area was 0.785 cm^2 . The D – E hysteresis loop measurements were carried

out at room temperature on a Premiere II ferroelectric tester from Radian Technologies, Inc., in combination with a Trek 10/10B-HS high voltage amplifier (0–10 kV AC, Lockport, NY, U.S.A.). The sample was immersed in a silicon oil bath during testing to avoid corona discharge in air. Similar as the BDS measurements, silver was evaporated onto both surfaces of the film as electrodes (50 nm thick), and the electrode area was about 0.0515 cm^2 .

Theoretical Background and Experimental Approaches. As illustrated in Scheme 1, a dielectric material can exhibit either linear or

Scheme 1. Illustration of Linear and Nonlinear Behavior for a Dielectric Material under a Cosine Driving Electric Field. The Right Panel Shows Both Linear and Nonlinear D – E Loops



nonlinear dielectric behavior under an input of a dynamic electric field at a constant temperature, T :

$$E(t) = E_0 \cos \omega t \quad (1)$$

where E_0 is the amplitude, ω the angular frequency ($\omega = 2\pi f$ with f being the frequency), and t time. For the linear dielectric, the output electric displacement $D(t)$ is still a cosine wave, but it lags behind $E(t)$ a phase angle, δ :²⁹

$$D(t) = D_a \cos(\omega t - \delta) \quad (2)$$

where D_a is the amplitude. The corresponding D – E loop is shown in the top right panel in Scheme 1. For a nonlinear dielectric, $D(t)$ not only lags behind $E(t)$, but also changes shape (see the bottom right panel in Scheme 1). As a result, $D(t)$ needs to be expressed as a Fourier series:³⁰

$$D(t) = D_0 + D_1(t) + D_2(t) + D_3(t) + D_4(t) + D_5(t) + \dots \quad (3)$$

where D_0 is the spontaneous electric displacement at zero electric field (i.e., spontaneous polarization P_0), $D_1(t)$ the linear component, and $D_n(t)$ ($n \geq 2$) the nonlinear components that account for the shape change. Note that P_0 is nonzero for a polarized sample, whereas it is zero for a nonpolarized sample because dipole moments from many dipoles/domains cancel one another. Because $D(t)$ lags behind $E(t)$, it can be decomposed into an in-phase wave $D'(t)$ and an out-of-phase wave $D''(t)$; $D(t) = D'(t) + D''(t)$. Accordingly, each linear and nonlinear term, $D_n(t)$, can also be decomposed into an in-phase wave $D'_n(t)$ and an out-of-phase wave $D''_n(t)$; $D_n(t) = D'_n(t) + D''_n(t)$. Each in-phase and out-of-phase component can be obtained as

$$D'_n(t) = D(t) \cos n\omega t \quad (4)$$

$$D''_n(t) = D(t) \sin n\omega t \quad (5)$$

The total in-phase [$D'(t)$] and out-of-phase [$D''(t)$] components can be obtained as

$$D'(t) = D_0 + D'_1(t) + D'_2(t) + D'_3(t) + D'_4(t) + D'_5(t) + \dots \quad (6)$$

$$D''(t) = D''_1(t) + D''_2(t) + D''_3(t) + D''_4(t) + D''_5(t) + \dots \quad (7)$$

By applying Fourier transformation (i.e., integration over a period, $Z = 1/f = 2\pi/\omega$) for both in-phase and out-of-phase components, we obtain the real and imaginary parts for D_n^* in a complex notion, $D_n^* = D'_n - iD''_n$:

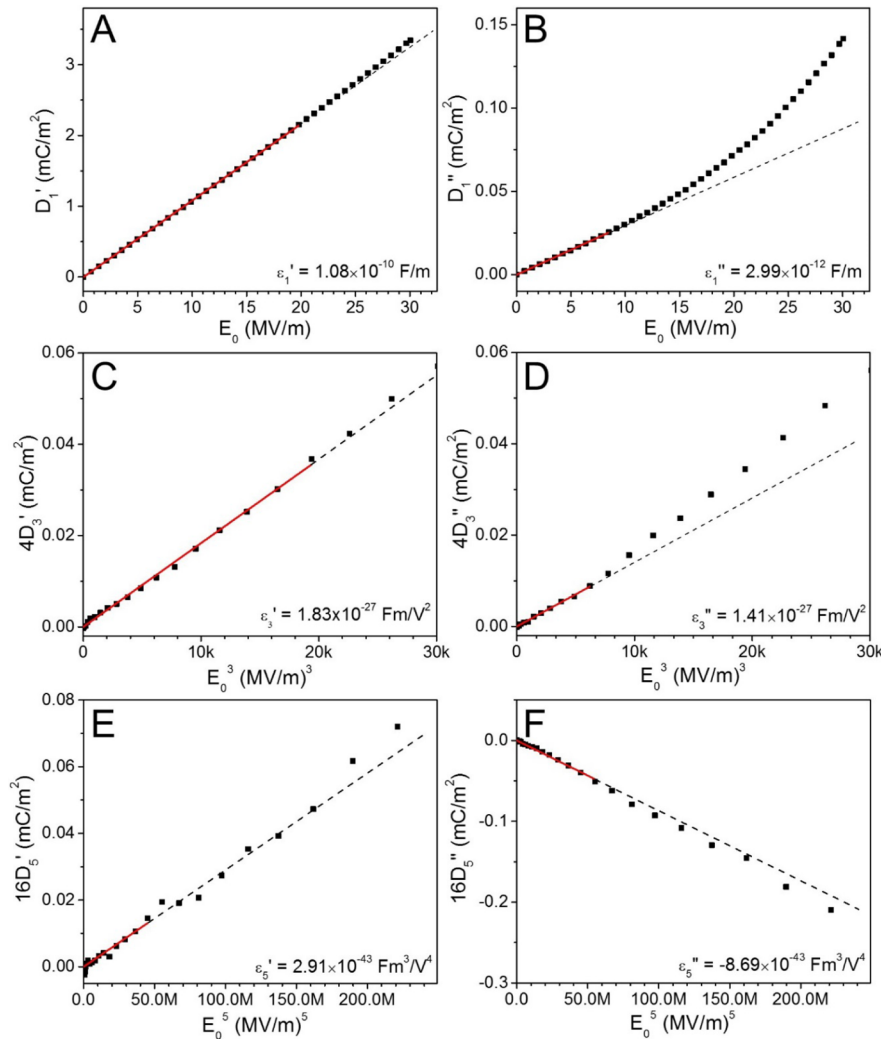


Figure 1. An example of method 1 to determine fundamental ϵ_n^* for the BOPVDF film: (A) D'_1 and (B) D''_1 versus E_0 , (C) $4D'_3$ and (D) $4D''_3$ versus E_0^3 , (E) $16D'_5$ and (F) $16D''_5$ versus E_0^5 at 25 °C and 0.1 Hz.

$$D_n^* = \frac{2}{Z} \int_0^Z D^*(t) \cos n\omega t dt \quad (8)$$

$$D_n'' = \frac{2}{Z} \int_0^Z D^*(t) \sin n\omega t dt \quad (9)$$

By using the definition of $D_n^* = \epsilon_n^* E_0$, we can also obtain complex apparent dielectric constant, ϵ_n^* ; $\epsilon_n^* = \epsilon'_n - i\epsilon''_n$. Since ϵ_n^* is the absolute permittivity defined by $\epsilon_n^* = \epsilon_m^* \epsilon_0$ (ϵ_0 is the vacuum permittivity), we can also obtain the complex relative permittivity: $\epsilon_m^* = \epsilon'_m - i\epsilon''_m$.

Alternatively, the electric displacement of a nonlinear dielectric material can be expressed as a Taylor series under both static and dynamic conditions:¹⁹

$$D = P_0 + D_1 + D_2 + D_3 + D_4 + D_5 + \dots \quad (10)$$

If we define $D_n = \epsilon_n E^n$, we can obtain

$$D = P_0 + \epsilon_1 E + \epsilon_2 E^2 + \epsilon_3 E^3 + \epsilon_4 E^4 + \epsilon_5 E^5 + \dots \quad (11)$$

Here, ϵ_1 is the fundamental linear dielectric constant, and ϵ_n ($n \geq 2$) is the fundamental nonlinear dielectric constant. Note that these Taylor terms in eqs 10 and 11 have nothing to do with those Fourier harmonics in eq 3. By applying a dynamic electric field, $E = E_0 \cos \omega t$, we obtain

$$\begin{aligned} D^*(t) = P_0 + \epsilon_1^* E_0 \cos \omega t + \epsilon_2^* E_0^2 \cos^2 \omega t + \epsilon_3^* E_0^3 \cos^3 \omega t \\ + \epsilon_4^* E_0^4 \cos^4 \omega t + \dots \quad (12) \end{aligned}$$

By applying Fourier transformation using eqs 8 and 9, we can get

$$D_0^* = P_0 + \frac{1}{2} \epsilon_2^* E_0^2 + \frac{3}{8} \epsilon_4^* E_0^4 + \dots \quad (13)$$

$$D_1^* = \epsilon_1^* E_0 + \frac{3}{4} \epsilon_3^* E_0^3 + \frac{10}{16} \epsilon_5^* E_0^5 + \dots \quad (14)$$

$$D_2^* = \frac{1}{2} \epsilon_2^* E_0^2 + \frac{1}{2} \epsilon_4^* E_0^4 + \frac{15}{32} \epsilon_6^* E_0^6 + \dots \quad (15)$$

$$D_3^* = \frac{1}{4} \epsilon_3^* E_0^3 + \frac{15}{16} \epsilon_5^* E_0^5 + \frac{21}{64} \epsilon_7^* E_0^7 + \dots \quad (16)$$

and so on. From eq 13, again $D_0^* = P_0$ when $E_0 = 0$. If E_0 is small enough, the higher components can be ignored, and thus the fundamental dielectric constants can be obtained for a nonlinear dielectric material:

$$\epsilon'_n = \lim_{E_0 \rightarrow 0} \frac{2^{n-1} D_n'}{E_0^n} \quad (17)$$

$$\epsilon''_n = \lim_{E_0 \rightarrow 0} \frac{2^{n-1} D_n''}{E_0^n} \quad (18)$$

From the above equations, ϵ'_n and ϵ''_n are fundamental dielectric constants and are thus independent upon the electric field (note that they still depend on frequency and temperature). On the contrary, the

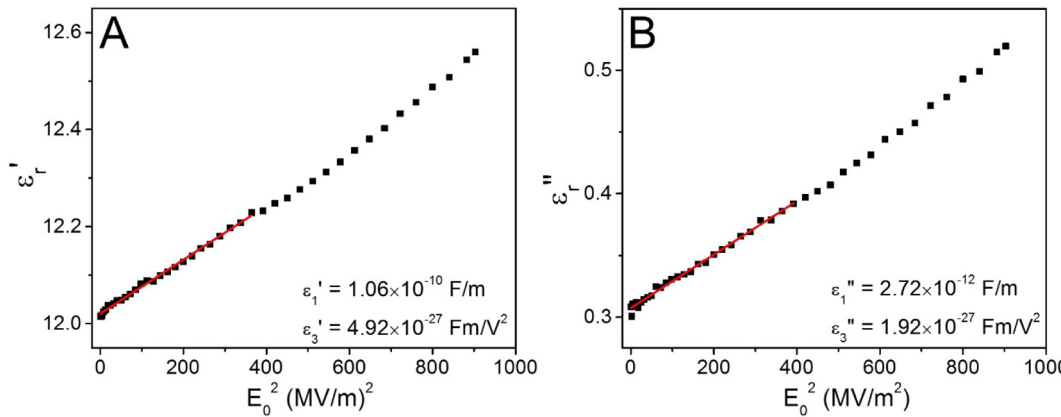


Figure 2. An example of method 2 to determine fundamental ϵ_n^* for the BOPVDF film: (A) ϵ'_r and (B) ϵ''_r versus E_0^2 at 25 °C and 0.1 Hz.

apparent dielectric constant ϵ_m^* is dependent on E_0 , f , and T . In general, if a sample does not possess spontaneous polarization P_0 (i.e., $P_0 = 0$), all even-numbered nonlinear dielectric constants will become zero because changing the polarity of the applied electric field will not be able to change the sign of the electric displacement D (e.g., see eq 15). On the contrary, if a sample possess a spontaneous polarization P_0 , the even-numbered nonlinear dielectric constants will be nonzero. For a ferroelectric semicrystalline polymer such as PVDF, ϵ'_r and ϵ''_r should represent the dipolar property of the amorphous phase plus the electronic/atomic polarization of both amorphous and crystalline phases because dipoles in the crystalline phase supposedly do not flip below the coercive field, E_C , which is about 70 MV/m for β PVDF crystals.^{19,31,32}

The main issue now is how to accurately measure D'_n and D''_n at low electric fields (e.g., below 15 MV/m). Furukawa and co-workers developed an accurate D - E loop instrument to apply a perfect sinusoidal electric field and then to determine both the linear term, D_1^* , and higher harmonics, D_n^* .¹⁹ By using this instrument, fundamental nonlinear dielectric constants up to the third harmonics (ϵ'_3 and ϵ''_3) at different frequencies and temperatures were determined for several dipolar polymers.^{14–16,20} However, other commercially available D - E loop testers (e.g., Radiant Technologies ferroelectric testers) have not been able to generate perfect sinusoidal electric fields, and thus they cannot be used to accurately determine the nonlinear dielectric properties for dipolar polymers. Recently, Novocontrol has developed a high voltage interface, HV4000, for broadband dielectric spectrometer (i.e., HVBDS) with ± 2000 V peak voltages and up to 10⁴ Hz switching frequency. In the following, we review its working mechanism and measure both fundamental and apparent nonlinear dielectric constants for a commercial BOPVDF film, which we have reported recently.²⁸

For HVBDS, the complex capacitance, C^* , for the sample is related to the measured complex current, I^* , under an applied sinusoidal voltage V :

$$C^* = -i \frac{I^*}{\omega V} - C_{\text{edge}} - C_s \quad (19)$$

where C_{edge} is the edge capacitance at the sample edge, and C_s is the stray capacitance from the instrument. Usually, for thin polymer films (e.g., $< 20 \mu\text{m}$) with a large test area ($> 3 \text{ cm}^2$), I^* is high enough, and thus C_{edge} and C_s can be neglected. Then, $C^* \approx -i \frac{I^*}{\omega V}$. By deconvoluting the I^* into a Fourier series, I_n^* , the C_n^* can be similarly obtained. From definition, the complex relative dielectric constants are related to the complex capacitances:

$$\epsilon_m^* = \frac{C_n^*}{C_0} \quad (20)$$

Note that in this series, nonlinear dielectric constants are the apparent nonlinear dielectric constants, not the fundamental nonlinear dielectric constants. Through ϵ_m^* , we shall be able to obtain D_n^* :

$$D_n^* = \epsilon_{r,n}^* E_0 \quad (\text{i. e.}, D'_n = \epsilon_{r,n}' E_0 \text{ and } D''_n = \epsilon_{r,n}'' E_0) \quad (21)$$

By plotting D'_n and D''_n versus E_0 , we will be able to obtain fundamental nonlinear dielectric constants, ϵ'_n and ϵ''_n , from slopes of the linear region at low electric fields using eqs 17 and 18. This method to determine fundamental dielectric constants is called method 1.

Alternatively, there is another method to determine fundamental nonlinear dielectric constants for samples with $P_0 = 0$. We call it method 2, as described below. Under extremely low electric fields, eq 11 can be expressed as the following by ignoring higher harmonics:

$$D^* = \epsilon_r^* \epsilon_0 E_0 \approx \epsilon_1^* E_0 + \epsilon_3^* E_0^3 \quad (22)$$

From eq 22, we obtain

$$\begin{aligned} \epsilon_r^* &= \frac{\epsilon_1^*}{\epsilon_0} + \frac{\epsilon_3^*}{\epsilon_0} E_0^2 \\ (\text{i. e.}, \epsilon_r') &= \frac{\epsilon_1'}{\epsilon_0} + \frac{\epsilon_3'}{\epsilon_0} E_0^2 \text{ and } \epsilon_r'' = \frac{\epsilon_1''}{\epsilon_0} + \frac{\epsilon_3''}{\epsilon_0} E_0^2 \end{aligned} \quad (23)$$

The HVBDS instrument can also measure the overall apparent dielectric constant ϵ_r^* without measuring the higher harmonics. By plotting ϵ'_r and ϵ''_r versus E_0^2 , we obtain ϵ'_1/ϵ'_3 and $\epsilon''_1/\epsilon''_3$ from the intercept and slope, respectively. In general, this method is less accurate than method 1 because it is established by ignoring higher harmonics.

RESULTS AND DISCUSSION

Determination of Fundamental Nonlinear Dielectric Constants. An example of method 1 to determine fundamental ϵ_n^* for the BOPVDF film is shown in Figure 1. The temperature was 25 °C, and the frequency was 0.1 Hz. At low E_0 values (<20 MV/m), ϵ_n^* could be obtained from the slopes of the linear portion of the curves. For example, ϵ'_1 and ϵ''_1 were 1.08×10^{-10} and 2.99×10^{-12} F/m, corresponding to relative dielectric constants of ϵ'_{r1} and ϵ''_{r1} being 12.2 and 0.34, respectively (the dissipation factor, $\tan \delta = 0.028$). ϵ'_3 and ϵ''_3 were 1.83×10^{-27} and 1.41×10^{-27} Fm/V². These values were similar to those determined for unpoled PVDF using the D - E loop instrument, that is, $\epsilon'_1 = 1.10 \times 10^{-10}$ F/m and $\epsilon'_3 = 3.47 \times 10^{-27}$ Fm/V².¹⁹ By using the HVBDS, we could also obtain ϵ'_s and ϵ''_s as shown in Figure 1, panels E and F. This was not possible from the D - E loop instrument.¹⁹ However, ϵ'_s and ϵ''_s became inaccurate when the frequency was above 3 Hz due to the instrument limit of accuracy under low electric fields. Therefore, we will primarily focus on the ϵ'_1 and ϵ'_3 for this study.

HVBDS could also measure overall ϵ'_r and ϵ''_r without any harmonics, and method 2 was used to determine the fundamental dielectric constants ϵ_1^* and ϵ_3^* . Figure 2, panels A and B show ϵ'_r and ϵ''_r versus E_0^2 at 25 °C and 0.1 Hz, respectively. As predicted in eq 23, a linear relationship was observed at low electric fields (<20 MV/m). From the intercept and slope (see eq 23), ϵ_1^* and ϵ_3^* were obtained, respectively.

To compare the accuracy of these two methods, the same procedures as in Figures 1 and 2 were adopted to determine ϵ_1^* and ϵ_3^* under various temperatures and frequencies. Corresponding results are shown in Figure 3. It was clear that the

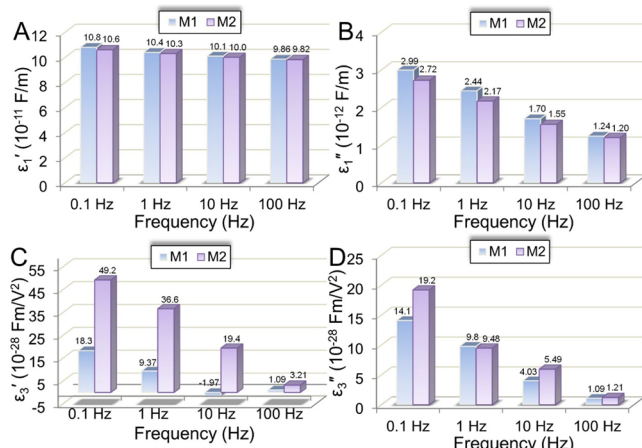


Figure 3. Comparison of methods 1 (M1) and 2 (M2) for determination of fundamental nonlinear dielectric constants, (A) ϵ'_r , (B) ϵ''_r , (C) ϵ'_3 , and (D) ϵ''_3 , under different frequencies at 25 °C.

fundamental linear dielectric constants (ϵ'_r and ϵ''_r) obtained from these two methods were fairly close to each other. However, the fundamental nonlinear dielectric constants (ϵ'_3 and ϵ''_3) determined by method 2 were generally larger than those determined by method 1. This could be attributed to the contributions from higher harmonics (i.e., ϵ_5^* , ϵ_7^* , and so on), which were ignored in method 2. Therefore, method 1 was chosen to study the nonlinear dielectricity of the BOPVDF film.

Origin of Nonlinear Dielectricity in BOPVDF under Low Electric Fields (<30 MV/m). By using method 1, the fundamental nonlinear dielectric constants for the BOPVDF film were determined at various temperatures and frequencies. Figure 4 shows ϵ'_1/ϵ''_1 , ϵ'_3/ϵ''_3 , and ϵ'_5/ϵ''_5 as a function of frequency between 25 and 75 °C. In Figure 4, panels A and B, the linear fundamental dielectric constants, ϵ'_1 and ϵ''_1 , decreased with increasing frequency and increased with increasing temperature. At 50 and 75 °C, the low frequency ϵ''_1 exhibited a slope close to -1 in the double logarithmic plot in Figure 4, panel B. From the literature, this could be explained by the migrational loss of impurity ions (i.e., subppm concentration) in BOPVDF.²⁸ In Figure 4, panels C and D, similar trends were observed for ϵ'_3 and ϵ''_3 . However, a significant difference was that both ϵ'_3 and ϵ''_3 became negligibly small or nearly zero above 10 Hz. Although the determined ϵ'_5 and ϵ''_5 values were not accurate, similar trends could also be observed in Figure 4, panels E and F. Namely, they also became nearly zero above 10 Hz. These results indicated that the low-field dielectric nonlinearity vanished for BOPVDF above 10 Hz. Given the fact that the relaxation frequency for amorphous PVDF dipoles was much higher than 10 Hz (i.e., around 1 MHz) at 25 °C,²⁸

the observed dielectric nonlinearity should not originate from dipolar relaxation of amorphous segments around the glass transition, as reported for PVAc and P(VDCN-VAc).^{14–16} Meanwhile, the bulk conductivity of the BOPVDF film at 25 °C was as low as 10^{-14} – 10^{-13} S/m;²⁸ therefore, the nonlinearity could not be attributed to electronic conduction. In addition, no ferroelectric switching of polar crystalline dipoles was possible when the electric field was below 30 MV/m. Therefore, we consider that the dielectric nonlinearity must originate from the migration (or conduction) of impurity ions in BOPVDF. As we can see from Figure 4, the higher the temperature and the lower the frequency, the more significant the ionic conduction and thus the dielectric nonlinearity. In other words, the fundamental dielectric nonlinearity for BOPVDF above room temperature should be an extrinsic (i.e., related to impurity ions), rather than an intrinsic, property of the BOPVDF film.

Nonlinear Dielectricity Associated with Ferroelectric Switching of Polar Crystalline Dipoles under High Electric Fields. When the electric field increased to beyond 30 MV/m, several physical events took place for the BOPVDF film. First, when the electric field increased to above 60–70 MV/m (i.e., the E_C), the 30% β crystalline dipoles started to flip, causing certain ferroelectricity. When the electric field increased to 100–150 MV/m, nonpolar α crystals would gradually transform into polar δ crystals.^{31–33} From further increasing the electric field to above 200–250 MV/m, the weakly polar δ crystals would transform into highly polar β crystals.^{31,32} In addition, increasing the poling time could also induce more $\alpha \rightarrow \delta$ and $\delta \rightarrow \beta$ phase transformations. These phase transformations would further enhance ferroelectricity of the BOPVDF film. According to our previous reports,²⁸ compared with ferroelectric dipole switching in the BOPVDF film, DC conduction and polarization of impurity ions should be negligible at room temperature.

The above-mentioned ferroelectric switching of polar crystalline dipoles/domains is nonlinear in nature. The high-field nonlinear dielectricity was studied by HVBDS. The results under various E_0 values at 25 °C are shown in Figure 5. From Figure 5, panels A and B, no obvious dipolar relaxation process in ϵ'_{r1} and ϵ''_{r1} was observed below 70 MV/m (i.e., the E_C), suggesting no ferroelectric switching of the β dipoles/domains in the sample. Above the E_C , obvious dipolar relaxation processes were observed in ϵ'_{r1} and ϵ''_{r1} . Below 20 Hz, ϵ'_{r1} showed high values (>25), and it decreased to 11–13 above 500 Hz. Similarly, ϵ''_{r1} showed high values below 20 Hz, and it decreased to about 1 above 500 Hz. The dissipation factor, $\tan \delta$, was as high as 0.4 below 20 Hz and about 0.08 above 1 kHz with no obvious relaxation peak observed (see Figure S1 in the Supporting Information). The stepwise decreases in ϵ'_{r1} and ϵ''_{r1} around 100 Hz with increasing frequency were thus attributed to ferroelectric switching of β (and some δ) dipoles/domains. Below 10 Hz, ϵ'_{r1} and ϵ''_{r1} exhibited gradual increases with decreasing frequency for E_0 between 70 and 170 MV/m. We speculate that it was because of continued phase transformation from the nonpolar α phase to the polar δ and β phases at long poling times.

From Figure 5, panels C and D, the apparent nonlinear dielectric constants, ϵ'_{r3} and ϵ''_{r3} , exhibited different behavior. First, when the E_0 was between 28 and 70 MV/m, the ϵ'_{r3} gradually increased with decreasing the poling frequency to below 20 Hz. This was attributed to the nonlinear behavior of impurity ions at low frequencies because the field was still

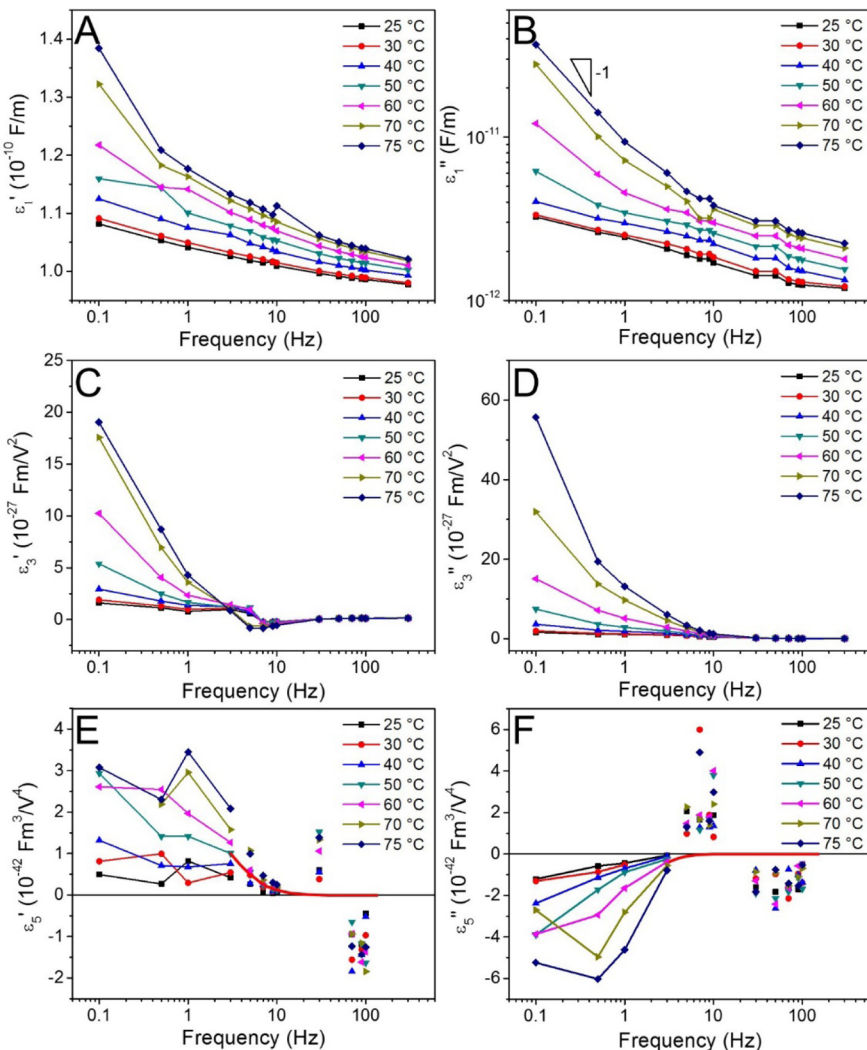


Figure 4. Fundamental dielectric constants for the BOPVDF film as a function of frequency at various temperatures: (A) ϵ'_1 , (B) ϵ''_1 , (C) ϵ'_3 , (D) ϵ''_3 , (E) ϵ'_5 , and (F) ϵ''_5 .

below the E_C . Second, when the E_0 was between 137 and 170 MV/m, $\epsilon'_{r,3}$ exhibited peak (i.e., either maximum or minimum) values around 10 Hz, suggesting again the flipping of β (and some δ) dipoles/domains. Finally, above 500 Hz, both $\epsilon'_{r,3}$ and $\epsilon''_{r,3}$ became zero, indicating the disappearance of dielectric nonlinearity because the frequency was too fast for crystalline dipoles to switch directions.

From the results in Figure 5, we can obtain D_n^* for the BOPVDF film under high electric fields, that is, $D_{n,\text{high}}^* = \epsilon_{r,n}^* \epsilon_0 E_0$. Note that the $D_{n,\text{high}}^*$ has contributions of dipolar and electronic/atomic polarizations from both crystalline and amorphous phases. If we want to obtain the nonlinear $P_{n,\text{cryst}}^*$ for pure PVDF crystals, from the $D_{n,\text{high}}^*$ we need to subtract dipolar polarization from amorphous dipoles and electronic/atomic polarizations from both crystalline and amorphous phases. As we mentioned earlier, the fundamental dielectric constants (ϵ_n^* , which is determined by HVBDS in Figure 4) account for the dipolar polarization from amorphous dipoles and electronic/atomic polarizations from both crystalline and amorphous phases at low electric fields. We shall be able to calculate the D_n^* from ϵ_n^* using eqs 14 and 16. Here, we call the D_n^* calculated from ϵ_n^* as $D_{n,\text{low}}^*$. By using HVBDS, however, we could only determine up to fifth harmonics of ϵ_n^* due to the

accuracy limit of the instrument. Therefore, we propose to ignore contributions from the seventh and above harmonics to estimate the $D_{n,\text{low}}^*$. Then the following relationship holds true:

$$\chi_c P_{n,\text{cryst}}^* = D_{n,\text{high}}^* - D_{n,\text{low}}^* \quad (24)$$

where χ_c is the volumetric crystallinity (48.2 vol %). In this way, we are able to obtain $P_{n,\text{cryst}}^*$ and the corresponding results at 10 Hz and 25 °C are shown in Figure 6. Note that ignoring the seventh and above harmonics of ϵ_n^* will introduce inaccuracy in $D_{n,\text{low}}^*$, especially at high electric fields, and we will discuss this later. From Figure 6, both $P'_{1,\text{cryst}}$ and $P''_{1,\text{cryst}}$ increased with increasing the E_0 , whereas $P'_{3,\text{cryst}}$ and $P''_{3,\text{cryst}}$ decreased to below zero at high electric fields.

By using this method, we were able to obtain $P_{1,\text{cryst}}^*$ and $P_{3,\text{cryst}}^*$ at different frequencies. Results for frequencies between 10 and 300 Hz are shown in Figure S2 in the Supporting Information. As we can see, both $P'_{1,\text{cryst}}$ and $P''_{1,\text{cryst}}$ decreased with increasing frequency, and $P'_{3,\text{cryst}}$ and $P''_{3,\text{cryst}}$ decreased to close to zero around 300 Hz. This result again indicated that ferroelectric switching of ferroelectric crystalline dipoles should disappear above 300 Hz.

As we mentioned above, ignoring the seventh and above harmonics of ϵ_n^* to calculate $D_{n,\text{low}}^*$ and thus $P_{n,\text{cryst}}^*$ will

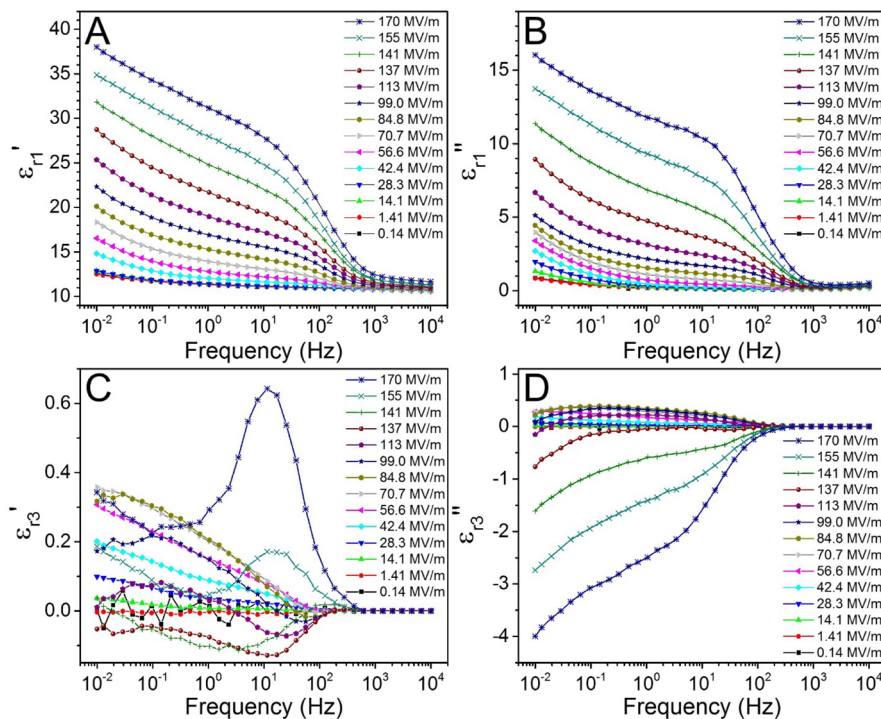


Figure 5. Apparent relative dielectric constants, (A) ϵ'_{r1} , (B) ϵ''_{r1} , (C) ϵ'_{r3} , and (D) ϵ''_{r3} , as a function of frequency under different E_0 at 25 °C.

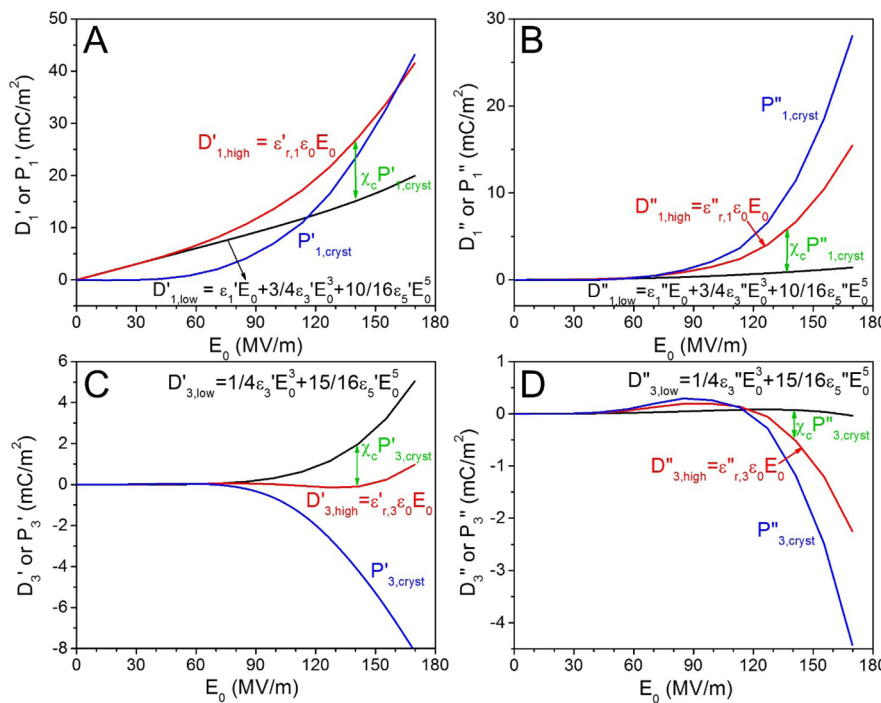


Figure 6. Calculation of $P_{n,\text{cryst}}^*$ (i.e., $(D_{n,\text{high}}^* - D_{n,\text{low}}^*)/\chi_c$) for PVDF crystals: (A) $P'_{1,\text{cryst}}$, (B) $P''_{1,\text{cryst}}$, (C) $P'_{3,\text{cryst}}$, and (D) $P''_{3,\text{cryst}}$. Here, $D_{n,\text{low}}^*$ is obtained using eqs 14 and 16 with up to fifth harmonics of the fundamental dielectric constant, ϵ_n^* . The $D_{n,\text{high}}^*$ is obtained by $D_{n,\text{high}}^* = \epsilon_{r,n}^* E_0$.

introduce significant errors, especially at high electric fields. In an alternative method, we used bipolar $D-E$ loops to obtain more accurate $P_{n,\text{cryst}}^*$. Bipolar $D-E$ loops for the BOPVDF film at 10 Hz and room temperature are shown in Figure 7, panel A. Again, compared with ferroelectric switching of polar crystalline dipoles/domains, ionic and DC conduction could be ignored, as shown in Section III in the Supporting Information. The total electric displacement of the BOPVDF film, D_{film} , included

contributions from electronic/atomic and dipolar polarizations of both amorphous and crystalline phases. To obtain the dipolar polarization from pure PVDF crystals, we needed to subtract the contributions from dipolar polarization, $(1 - \chi_c) P_{\text{dip}}^{\text{am}}$, of the amorphous dipoles and electronic/atomic polarizations ($D_{e/a}^{\text{film}}$) of both amorphous and crystalline phases (i.e., $D_{e/a}^{\text{film}} + (1 - \chi_c) P_{\text{dip}}^{\text{am}}$, which we call it deformational electric displacement ($D_{\text{def}}^{\text{film}}$)) because these polarization mechanisms

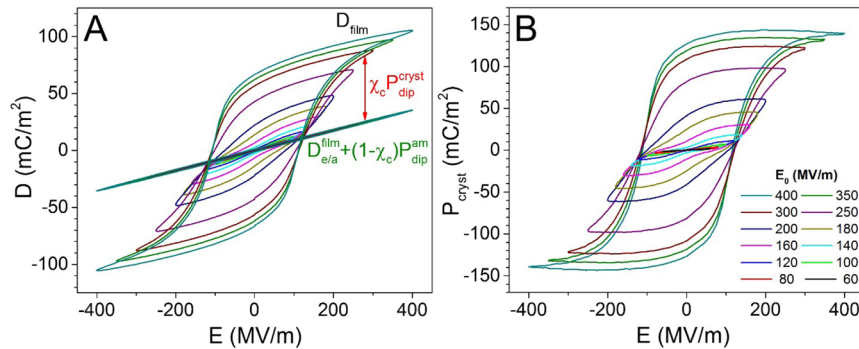


Figure 7. (A) Bipolar D – E loops for the BOPVDF film at room temperature, showing typical ferroelectric switching of polar crystalline dipoles/domains. The poling frequency is 10 Hz with a sinusoidal wave function. Extracted deformational D – E loops (i.e., without ferroelectric switching of crystalline dipoles) are also shown (see Section III in the Supporting Information for the detailed extraction method). (B) Calculated bipolar P – E loops for pure PVDF crystals in the BOPVDF film.

should not exhibit losses at 10 Hz and room temperature). Note that $D_{\text{def}}^{\text{film}}$ cannot be directly measured for the neat BOPVDF film because of ferroelectric switching of polar crystalline dipoles above the E_C at 70 MV/m. However, it has been reported previously that ferroelectric switching of polar crystalline dipoles can be effectively stopped in polycarbonate (PC)/PVDF multilayer films.²⁵ In this study, we extracted the $D_{\text{def}}^{\text{film}}$ using a PC/PVDF bilayer film coextruded previously,²⁵ and the extraction details are shown in Section IV in the Supporting Information. The extracted deformational D – E loops for PVDF are shown in Figure 7, panel A. After subtraction, we could obtain the bipolar P – E loops for pure PVDF crystals by

$$\chi_c P_{\text{dip}}^{\text{cryst}} = D_{\text{film}} - (1 - \chi_c) P_{\text{dip}}^{\text{am}} \quad (25)$$

The subtracted P – E loops for the pure PVDF crystals are shown in Figure 7, panel B. Obvious rectangular hysteresis loops were observed at E_0 above 200 MV/m. The maximum polarization reached about 140 mC/m² at 400 MV/m. Such a high maximum polarization suggested that continuous poling of the BOPVDF film to 400 MV/m could transform a significant amount of α crystals into β crystals. Below 200 MV/m, double hysteresis loops were observed, which could be attributed to a stronger depolarization field than the polarization field when the poling field was low, as we reported before.^{34,35}

From the subtracted P – E loops in Figure 7, panel B, we obtained $P_{\text{dip}}^{\text{cryst}}(t)$ waves as a function of time in a period (100 ms); see Figure 8. Obviously, the $P_{\text{dip}}^{\text{cryst}}(t)$ lagged behind the driving electric field $E(t)$. In addition, the waveform gradually transformed from more a sinusoidal shape into a square shape as the E_0 increased to above 200 MV/m, indicating the nonlinear response of polar PVDF crystals.

From the $P_{\text{dip}}^{\text{cryst}}(t)$ waves in Figure 8, we obtained accurate $P_{n,\text{cryst}}^*$ and thus $\epsilon_{rn,\text{cryst}}^*$ for polar PVDF crystals. The corresponding results are shown in Figure 9. Below 140 MV/m, $P_{3,\text{cryst}}^* - P_{7,\text{cryst}}^*$ exhibited fairly small values (Figure 9C–F), suggesting weak nonlinearity because most PVDF crystals were still mostly in the nonpolar α crystals. At 60 MV/m, the overall linear dielectric constant for the PVDF crystals, that is, $|e_{r1}^*| = [(\epsilon'_{r1,\text{cryst}})^2 + (\epsilon''_{r1,\text{cryst}})^2]^{1/2}$, was only 3.84 (Figure 9A), much smaller than that (ca. 21) estimated for the amorphous PVDF phase in the BOPVDF film.²⁸ With further increasing the electric field to 400 MV/m, the $|e_{r1}^*|$ for the pure PVDF crystals gradually increased to about 50. Meanwhile, the nonlinear dielectric constants, $\epsilon_{r3}^* - \epsilon_{r7}^*$ became more significant above

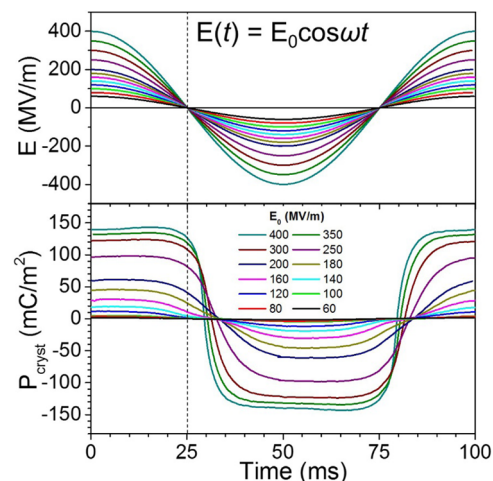


Figure 8. Dynamic driving electric field (E) and the resulting $P_{\text{dip}}^{\text{cryst}}$ (obtained from Figure 7B) as a function of time for various E_0 values.

300 MV/m in Figure 9, panels C–F, indicating the nonlinear nature of ferroelectric switching of a large amount of β dipoles (which included those transformed from the α/δ phases) in the polarized sample. The results for $P_{n,\text{cryst}}^*$ in Figure 9 were generally consistent with the simulated nonlinear dielectric properties for PVDF based on the Preisach model.³⁶ Figure 9, panels A–D also compared $\epsilon_{r1,\text{cryst}}^*$ and $\epsilon_{r3,\text{cryst}}^*$ values obtained from D – E loop and HBVDS measurements. Obviously, the results from HBVDS became increasingly inaccurate at >100 MV/m because we had ignored greater than seventh harmonics of ϵ_n^* during the calculation of $D_{n,\text{low}}^*$.

Intrinsic Relaxation Behavior of Polar Crystalline Dipoles at Various Temperatures. Compared to the D – E loop test, HBVDS has an advantage of fast and comprehensive investigation of nonlinear dielectric properties for polar polymers, covering a broad range of electric field, frequency, and temperature. Figure 10 shows the overall apparent dielectric constants, ϵ'_r and ϵ''_r (obtained by not measuring the higher harmonics as in method 2 mentioned above), as a function of frequency for the BOPVDF film at various electric fields and temperatures. At -90°C (i.e., below the T_g ; see Figure 10A), the ϵ'_r was around 3.5–4 between 10^{-2} and 10^4 Hz when the E_0 was below 70 MV/m because both amorphous and crystalline dipoles were largely frozen. Above 85 MV/m, ϵ'_r gradually increased with decreasing the frequency below 1 kHz. This trend became more obvious at high electric fields. This

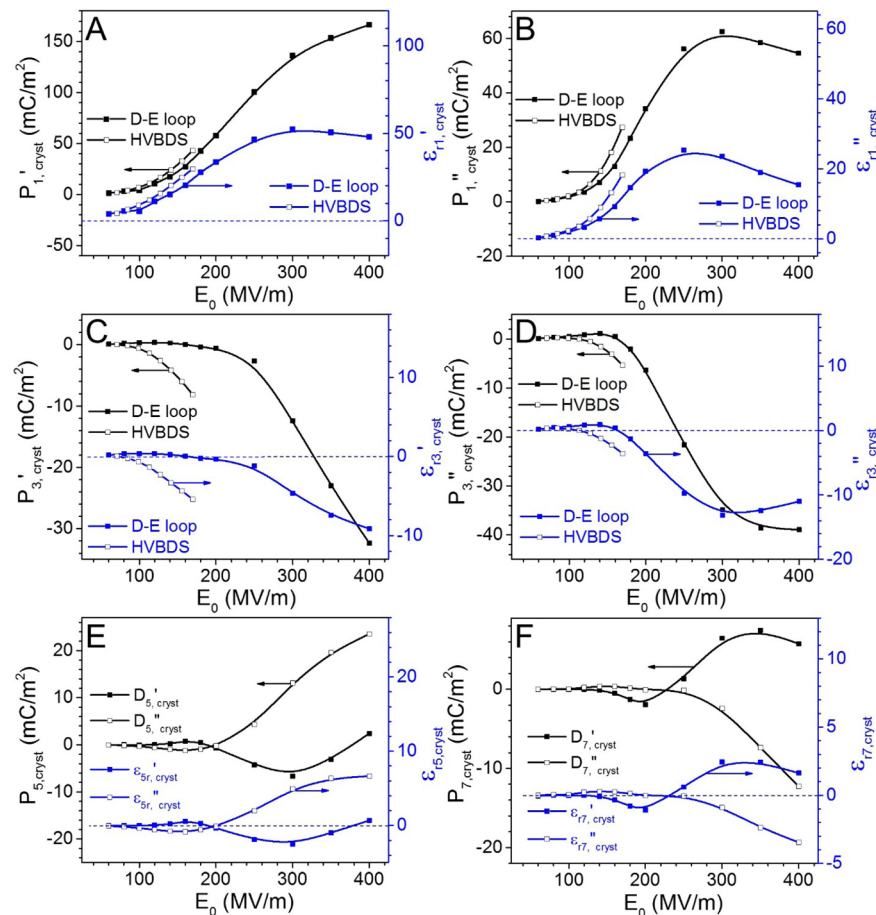


Figure 9. (A) $P'_{1,\text{cryst}}/\epsilon'_{r1,\text{cryst}}$, (B) $P''_{1,\text{cryst}}/\epsilon''_{r1,\text{cryst}}$, (C) $P'_{3,\text{cryst}}/\epsilon'_{r3,\text{cryst}}$, (D) $P''_{3,\text{cryst}}/\epsilon''_{r3,\text{cryst}}$, (E) $P^*_{5,\text{cryst}}/\epsilon^*_{r5,\text{cryst}}$, and (F) $P^*_{7,\text{cryst}}/\epsilon^*_{r7,\text{cryst}}$ as a function of E_0 at 10 Hz and room temperature.

increase in ϵ'_r at low frequencies could be attributed to the flipping of a small fraction of crystalline dipoles under high fields because the amorphous PVDF dipoles were frozen. Above the T_g there was a clear relaxation process between 30 and 1000 Hz (see Figure 10B–F), which could be attributed to the ferroelectric switching of polar crystalline dipoles/domains in concert with the switching of the amorphous dipoles. Intriguingly, the ferroelectric switching appeared to be independent upon temperature. This behavior was completely different from that of amorphous dipoles, whose relaxation frequency intimately depended on temperature via either the Vogel–Tamman–Fulcher (VTF) (close to T_g) or the Arrhenius (much higher than T_g) equation.³⁷ With increasing the temperature, the low frequency ϵ'_r gradually increased, accompanied by a gradual increase in the ϵ'_r (i.e., loss) as well, indicating stronger dipolar interactions due to enhance dipole mobility in both amorphous and crystalline phases. When the temperature was above 50 °C, the low frequency ϵ'_r substantially increased when the E_0 was below the E_C of 70 MV/m (Figure 10E,F). This could be attributed to the migrational loss from impurity ions in the sample. Above 85 MV/m (or above the E_C), the loss from impurity ions became less significant, suggesting that polarization of crystalline dipoles in PVDF crystals could significantly affect the mobility of impurity ions in the amorphous phase. On the basis of our previous reports,^{34,35} polarized crystalline dipoles in PVDF crystals could strongly interact with the nearby amorphous dipoles. In turn, the aligned amorphous dipoles would create a

depolarization (or reverse) field to decrease the local electric field and thus decrease the mobility of impurity ions in the amorphous phase. This would explain the reduced low frequency ϵ''_r at 100 °C when the E_0 was above 85 MV/m (Figure 10F) as compared to the cases where the E_0 was between 14 and 42 MV/m. Finally, the dissipation factor, $\tan \delta$, results are shown in Figure S6 in the Supporting Information.

CONCLUSIONS

In summary, HVBDS is an effective and accurate way to measure both fundamental and apparent nonlinear dielectric constants for polar polymers under a broad range of electric field, frequency, and temperature. In this study, nonlinear dielectric properties of a commercial BOPVDF film with 48 vol % crystallinity (ca. 70% α phase and 30% β phase) were studied. Under low electric fields (i.e., below the E_C), only electronic/atomic polarizations in the sample and dipolar polarization from the amorphous dipoles contributed to the dielectric property because crystalline dipoles were not yet mobile. The linear fundamental dielectric constants, ϵ^*_1 , increased with increasing temperature and decreasing frequency because of enhanced dipolar interactions among amorphous PVDF dipoles.^{28,38} However, nonlinear fundamental dielectric constants, ϵ^*_3 and ϵ^*_5 , vanished above 10 Hz, suggesting that the nonlinear fundamental dielectric constants must origin from impurity ions rather than from the amorphous PVDF dipoles. In other words, if impurity ions can be completely eliminated,

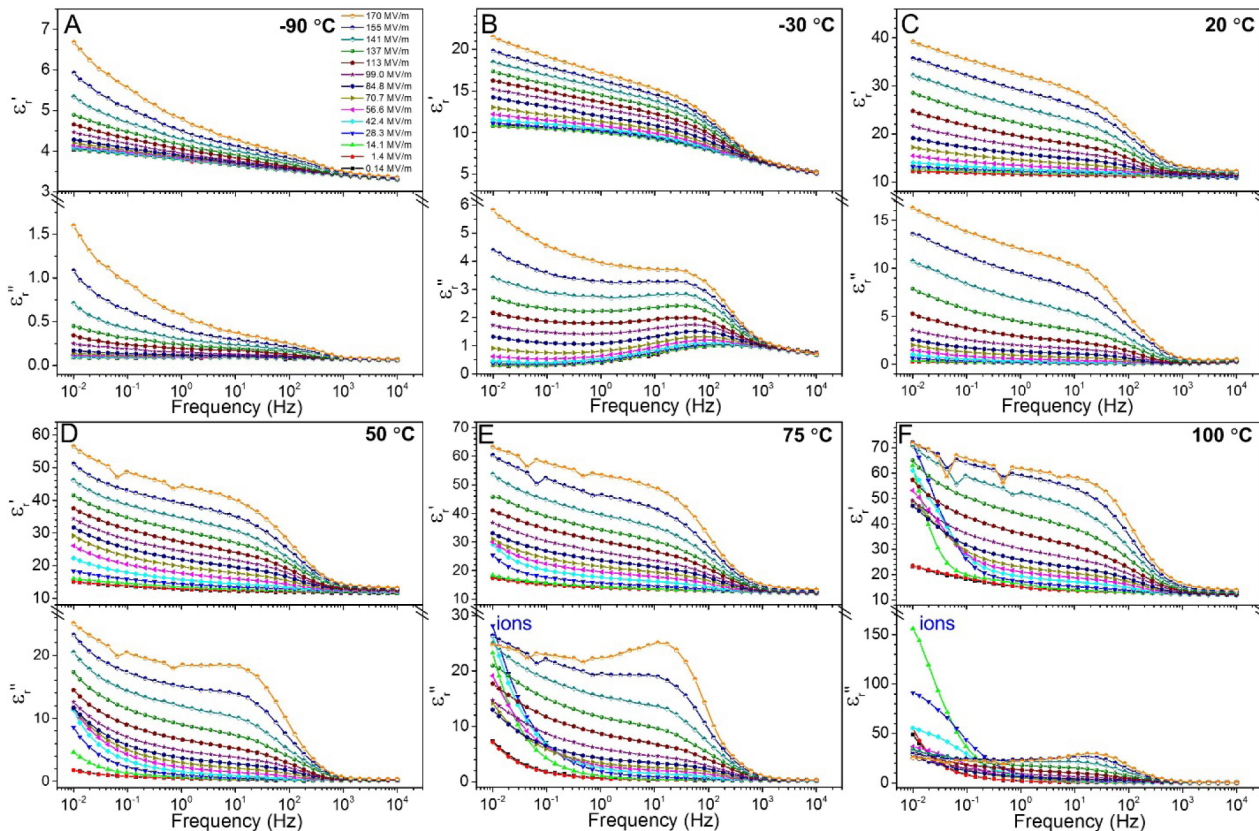


Figure 10. Real (ϵ') and imaginary (ϵ'') parts of relative permittivity as a function of frequency for the BOPVDF film at various electric fields (0.14–170 MV/m) and temperatures: (A) $-90\text{ }^{\circ}\text{C}$, (B) $-30\text{ }^{\circ}\text{C}$, (C) $20\text{ }^{\circ}\text{C}$, (D) $50\text{ }^{\circ}\text{C}$, (E) $75\text{ }^{\circ}\text{C}$, and (F) $100\text{ }^{\circ}\text{C}$.

PVDF should behave as a linear dielectric at room temperature when the electric field is below the E_C .

Above the E_C , polar crystalline dipoles/domains started to flip, resulting in nonlinear ferroelectricity. To determine nonlinear dipolar polarization for pure PVDF crystals, contributions from electronic/atomic polarizations of the sample and the dipolar polarization of the amorphous phase needed to be subtracted. Experimental results showed that the $D-E$ loop method was more accurate than the HVBDS method, where higher than seventh harmonics of ϵ_n^* were ignored during the calculation introducing significant errors at high fields. Nonetheless, HVBDS was convenient to study apparent nonlinear dielectric constants under a broad range of electric field, temperature, and frequency. It was intriguing to observe that the relaxation of ferroelectric PVDF crystals always took place between 10 and 500 Hz regardless of different temperatures and electric fields.

From this study, we understand that amorphous PVDF dipoles do not cause dielectric nonlinearity, whereas impurity ions and polar crystalline dipoles do. To utilize PVDF for high energy density and low loss dielectric films, nonlinearity from impurity ions and polar crystalline dipoles must be avoided. On the basis of our recent reports,^{25,26} PVDF-based multilayer films (multilayering with PC) are an effective way to reduce migrational loss from impurity ions and prevent ferroelectric dipole switching at the same time.

ASSOCIATED CONTENT

Supporting Information

The Supporting Information is available free of charge on the ACS Publications website at DOI: [10.1021/acsami.5b09368](https://doi.org/10.1021/acsami.5b09368).

Dissipation factors for the BOPVDF film at different temperatures, calculated $P_{n,\text{cryst}}^*$ versus frequency for pure PVDF crystals by HVBDS, influence of free charge polarization under high electric fields, extraction of deformational $D-E$ loops for PVDF, and high-field dissipation factors at different temperatures (PDF)

AUTHOR INFORMATION

Corresponding Authors

*Phone: +1 216-368-5861. Fax: +1 216-368-4202. E-mail: lzx121@case.edu.

*E-mail: jxw319@cqu.edu.cn.

Notes

The authors declare no competing financial interest.

ACKNOWLEDGMENTS

This work is supported by National Science Foundation (DMR-1402733). Y.L. and J.W. acknowledge financial support from China Scholarship Council. Partial support from the National Natural Science Foundation of China (Grant No. S1528302) is also acknowledged. The HVBDS instrument is supported by Army Research Office (ARO) under Award No. W911NF-13-1-0153.

REFERENCES

- Zhu, L. Exploring Strategies for High Dielectric Constant and Low Loss Polymer Dielectrics. *J. Phys. Chem. Lett.* **2014**, *5*, 3677–3687.
- Sarjeant, W. J.; Zirnheld, J.; MacDougall, F. W. Capacitors. *IEEE Trans. Plasma Sci.* **1998**, *26*, 1368–1392.

- (3) Facchetti, A.; Yoon, M. H.; Marks, T. J. Gate Dielectrics for Organic Field-Effect Transistors: New Opportunities for Organic Electronics. *Adv. Mater.* **2005**, *17*, 1705–1725.
- (4) Ortiz, R. P.; Facchetti, A.; Marks, T. J. High-k Organic, Inorganic, and Hybrid Dielectrics for Low-Voltage Organic Field-Effect Transistors. *Chem. Rev.* **2010**, *110*, 205–239.
- (5) Pelrine, R.; Kornbluh, R.; Joseph, J.; Heydt, R.; Pei, Q. B.; Chiba, S. High-Field Deformation of Elastomeric Dielectrics for Actuators. *Mater. Sci. Eng., C* **2000**, *11*, 89–100.
- (6) Brochu, P.; Pei, Q. Advances in Dielectric Elastomers for Actuators and Artificial Muscles. *Macromol. Rapid Commun.* **2010**, *31*, 10–36.
- (7) Zhang, Q. M.; Bharti, V.; Zhao, X. Giant Electrostriction and Relaxor Ferroelectric Behavior in Electron-Irradiated Poly(vinylidene fluoride-trifluoroethylene) Copolymer. *Science* **1998**, *280*, 2101–2104.
- (8) Zhang, Q. M.; Huang, C.; Xia, F.; Su, J. Electric EAP. In *Electroactive Polymer (EAP) Actuators as Artificial Muscles: Reality, Potential, and Challenges*, 2nd ed.; Bar-Cohen, Y., Ed.; SPIE Press, 2004; Chapter 4, pp 89–139.
- (9) Lu, S.-G.; Zhang, Q. Electrocaloric Materials for Solid-State Refrigeration. *Adv. Mater.* **2009**, *21*, 1983–1987.
- (10) Moya, X.; Kar-Narayan, S.; Mathur, N. D. Caloric Materials near Ferroic Phase Transitions. *Nat. Mater.* **2014**, *13*, 439–450.
- (11) Montanari, D.; Saarinen, K.; Scagliarini, F.; Zeidler, D.; Niskala, M.; Nender, C. Film Capacitors for Automotive and Industrial Applications. *Proceedings of CARTS U.S.A. 2009*; Jacksonville, FL, March 30–April 2, 2009.
- (12) Wen, H.; Xiao, W.; Wen, X.; Armstrong, P. Analysis and Evaluation of DC-Link Capacitors for High-Power-Density Electric Vehicle Drive Systems. *IEEE Trans. Veh. Technol.* **2012**, *61*, 2950–2964.
- (13) Zhu, L.; Wang, Q. Novel Ferroelectric Polymers for High Energy Density and Low Loss Dielectrics. *Macromolecules* **2012**, *45*, 2937–2954.
- (14) Furukawa, T. Nonlinear Dielectric Relaxations of Polymers. *J. Non-Cryst. Solids* **1991**, *131-133*, 1154–1157.
- (15) Furukawa, T.; Matsumoto, K. Nonlinear Dielectric-Relaxation Spectra of Polyvinyl Acetate. *Jpn. J. Appl. Phys.* **1992**, *31*, 840–845.
- (16) Furukawa, T.; Tada, M.; Nakajima, K.; Seo, I. Nonlinear Dielectric Relaxations in a Vinylidene Cyanide Vinyl-Acetate Copolymer. *Jpn. J. Appl. Phys.* **1988**, *27*, 200–204.
- (17) Bauer, S.; Bauer-Gogonea, S.; Ploss, B.; Ploss, B. Nonlinear Dielectric Response of Poled Amorphous Polymer Dipole Glasses. *J. Non-Cryst. Solids* **2005**, *351*, 2759–2763.
- (18) Furukawa, T.; Lovinger, A. J.; Davis, G. T.; Broadhurst, M. G. Dielectric Hysteresis and Nonlinearity in a 52/48 mol% Copolymer of Vinylidene Fluoride and Trifluoroethylene. *Macromolecules* **1983**, *16*, 1885–1890.
- (19) Furukawa, T.; Nakajima, K.; Koizumi, T.; Date, M. Measurements of Nonlinear Dielectric in Ferroelectric Polymers. *Jpn. J. Appl. Phys.* **1987**, *26*, 1039–1045.
- (20) Kodama, H.; Takahashi, Y.; Furukawa, T. Nonlinear Dielectric Investigation of Trifluoroethylene Rich Copolymers of Vinylidene Fluoride. *Jpn. J. Appl. Phys.* **1999**, *38*, 3589–3595.
- (21) Furukawa, T.; Saito, Y.; Tsutsumi, Y. *Nonlinear Dielectric Investigation of Ferroelectric Liquid Crystals*. 7th International Symposium on Electrets (ISE 7): Proceedings: Berlin, Germany, September 25, 1991; pp 421–426.
- (22) Tajitsu, Y. Linear and Non-linear Dielectric Spectroscopy of Polymeric Ferroelectric Liquid Crystals. *J. Mater. Sci. Lett.* **1998**, *17*, 989–992.
- (23) Ploss, B.; Ploss, B. Dielectric Nonlinearity of PVDF-TrFE Copolymer. *Polymer* **2000**, *41*, 6087–6093.
- (24) Wang, X.; Nelson, J. K.; Schadler, L. S.; Hillborg, H. Mechanisms Leading to Nonlinear Electrical Response of a Nano *p*-SiC/Silicone Rubber Composite. *IEEE Trans. Dielectr. Electr. Insul.* **2010**, *17*, 1687–1696.
- (25) Mackey, M.; Schuele, D. E.; Zhu, L.; Flandin, L.; Wolak, M. A.; Shirk, J. S.; Hiltner, A.; Baer, E. Reduction of Dielectric Hysteresis in Multi layered Films via Nanoconfinement. *Macromolecules* **2012**, *45*, 1954–1962.
- (26) Mackey, M.; Schuele, D. E.; Zhu, L.; Baer, E. Layer Confinement Effect on Charge Migration in Polycarbonate/Poly(vinylidene fluoride-co-hexafluoropropylene) Multilayered Films. *J. Appl. Phys.* **2012**, *111*, 113702.
- (27) Tseng, J. K.; Tang, S.; Zhou, Z.; Mackey, M.; Carr, J. M.; Mu, R.; Flandin, L.; Schuele, D. E.; Baer, E.; Zhu, L. Interfacial Polarization and Layer Thickness Effect on Electrical Insulation in Multilayered Polysulfone/Poly(vinylidene fluoride) Films. *Polymer* **2014**, *55*, 8–14.
- (28) Yang, L.; Ho, J.; Allahyarov, E.; Mu, R.; Zhu, L. Semicrystalline Structure - Dielectric Property Relationship and Electrical Conduction in a Biaxially Oriented Poly(vinylidene fluoride) Film under High Electric Fields and High Temperatures. *ACS Appl. Mater. Interfaces* **2015**, *7*, 19894–19905.
- (29) Blythe, A. R.; Bloor, D. *Electrical Properties of Polymers*, 2nd ed.; Cambridge University Press: New York, 2005.
- (30) Boashash, B. *Time Frequency Signal Analysis and Processing: A Comprehensive Reference*, 1st ed.; Elsevier: Boston, 2003.
- (31) Lovinger, A. J. Ferroelectric Polymers. *Science* **1983**, *220*, 1115–1121.
- (32) Tashiro, K. Crystal Structure and Phase Transition of PVDF and Related Copolymers. In *Ferroelectric Polymers: Chemistry, Physics, and Applications*, 1st ed.; Nalwa, H. S., Ed.; Marcel Dekker: New York, 1995; Chapter 2, pp 63–182.
- (33) Li, M.; Wondergem, H. J.; Spijkman, M. J.; Asadi, K.; Katsouras, I.; Blom, P. W. M.; de Leeuw, D. M. Revisiting the δ -Phase of Poly(vinylidene fluoride) for Solution-Processed Ferroelectric Thin Films. *Nat. Mater.* **2013**, *12*, 433–438.
- (34) Guan, F.; Wang, J.; Pan, J.; Wang, Q.; Zhu, L. Effects of Polymorphism and Crystallite Size on Dipole Reorientation in Poly(vinylidene fluoride) and Its Random Copolymers. *Macromolecules* **2010**, *43*, 6739–6748.
- (35) Guan, F.; Wang, J.; Yang, L.; Tseng, J.-K.; Han, K.; Wang, Q.; Zhu, L. Confinement-Induced High-Field Antiferroelectric-like Behavior in a Poly(vinylidene fluoride-co-trifluoroethylene-co-chlorotrifluoroethylene)-graft-polystyrene Graft Copolymer. *Macromolecules* **2011**, *44*, 2190–2199.
- (36) Tsang, C. H.; Shin, F. G. Simulation of Nonlinear Dielectric Properties of Polyvinylidene Fluoride Based on the Preisach Model. *J. Appl. Phys.* **2003**, *93*, 2861–2865.
- (37) Kremer, F.; Schönhals, A. *Broadband Dielectric Spectroscopy*; Springer: New York, 2003.
- (38) Karasawa, N.; Goddard, W. A. III Force Fields, Structures, and Properties of Poly(vinylidene fluoride) Crystals. *Macromolecules* **1992**, *25*, 7268–7281.